PAPER

Check for updates

Engineering pore nanospaces by introducing aromatic effects in UiO-66 for efficient separation of light hydrocarbons†

Liang Zhang, Xiao-Hong Xiong, Liu-Li Meng, Lu-Zhu Qin, Cheng-Xia Chen, [ID] Zhang-Wen Wei [ID] * and Cheng-Yong Su [ID] *

Natural gas, as one of the most widely used clean energies, has attracted significant attention due to its abundance, safe nature, and low cost but requires further separation and purification to produce downstream commodities more efficiently. In this case, the simultaneous removal of ethane and propane from natural gas is very important but challenging due to their similar physical and chemical properties. Herein, a pore-nanospace-engineering strategy was developed to construct a series of UiO-66-type zirconium MOFs by introducing different aromatic linkers, *i.e.*, UiO-66, UiO-66-Naph, DUT-52 and UiO-66-Anth, for natural gas separation and purification, revealing that the appropriate aromatic effect plays a vital role in the separation of the ternary $C_3H_8/C_2H_6/CH_4$ gas mixture. Specifically, UiO-66-Naph exhibited the best C_2/C_3 (C_2H_6 and C_3H_8) light hydrocarbon separation potential from CH_4, indicating that the introduction of naphthalene moieties not only effectively reduced the pore size but also provided a suitable aromatic pore-environment for C_2H_6/C_3H_8-framework interactions through dispersion and induction forces, which was corroborated by theoretical calculations and transient breakthrough experiments.

10th anniversary statement

On the occasion of the 10th anniversary of Journal of Materials Chemistry A, it is my great honour and pleasure to dedicate this work. Since 2010, I have been an Advisory Board member of Journal of Materials Chemistry. I have been involved in this journal and later Journal of Materials Chemistry A and enjoyed the service and knowledge acquisition in this community and contributed 50 publications. As one of my most favourite journal series, the Journal of Materials Chemistry family always attracts me because of its high-quality works, covering wide interdisciplinary fields in materials chemistry, especially the materials relevant to energy, catalysis, sensors and gas adsorption applications, which I am particularly interested in.

1. Introduction

Nowadays, the increasing severity of energy crisis and environmental pollution seriously threaten human survival and development together with the growth of global economy, owing to the burning of large amounts of fossil fuels.[1,2] Therefore, it is essential to explore new clean energy sources as an alternative to the traditional fossil fuels, such as coal and oil. In this respect, natural gas, as a type of abundant energy, has presented great potential in the chemical industry and daily life, mainly because of its abundance, high calorific value, low air pollution

(NO$_x$, SO$_2$, and smoke/particle), and low carbon dioxide emissions.[3–5]

It is well known that natural gas is mainly composed of CH_4 (75–90%), C_2H_6 (0–20%), C_3H_8 (0.01–5%), and small amount of impurities (H_2S, CO_2, N_2, water vapor, *etc.*).[6–8] Notably, CH_4 is not only a promising energy alternative but also an important chemical feedstock for the production of various downstream commodities.[3,4,9] Additionally, C_2H_6 and C_3H_8 are important raw materials in the chemical industry.[5,10,11] However, a small amount of C_2H_6 and C_3H_8 impurities can have serious influence on the conversion rate of CH_4, cyclic steady state, and safety in CH_4 storage, transportation, and utilization.[12–14] Hence, it is highly indispensable to realize the efficient separation of C_2H_6 and C_3H_8 over CH_4 from an industrial viewpoint.

The industrial separation of low-concentration C_2–C_3 light hydrocarbons from CH_4 usually relies on cryogenic distillation technology at high pressure and low temperature, resulting in high cost and energy footprint penalty.[15–17] Therefore, the development of cost- and energy-effective separation technology

12902 | *J. Mater. Chem. A*, 2023, 11, 12902–12909

This journal is © The Royal Society of Chemistry 2023

is of great importance.[18,19] Recently, nonthermal-driven adsorption separation technology based on porous solid materials has attracted significant attention owing to its low cost and energy efficiency.[20–25]

Due to their high surface areas, designable structures and tunable functionalities, metal–organic frameworks (MOFs), as a class of porous solid materials constructed with metal ions/clusters and organic ligands through coordination bonds, have shown great potential in gas adsorption and separation.[26–31] Among them, zirconium-based MOFs (Zr-MOFs) constructed with strong Zr–O bonds have been intensively exploited on account of their high thermal and chemical stability, which bestow them with great practical application potential in gas adsorption and separation. In particular, the UiO-66 family, constructed from saturatedly coordinated Zr-clusters and derivatives of terephthalic acid, has become a type of representative Zr-MOFs. A prerequisite for the effective separation of C_2–C_3 light hydrocarbons from CH_4 based on MOFs is elaborate manipulation of their pore system because of the similar molecular size and chemical property of $CH_4/C_2H_6/C_3H_8$, especially C_2H_6/CH_4.[32] To date, tremendous efforts have been devoted to developing highly effective MOF adsorbents through various strategies for purifying CH_4 from a binary C_2H_6/CH_4 or C_3H_8/CH_4 gas mixture. However, the simultaneous removal of both C_2H_6 and C_3H_8 from ternary gases mixture in a one-step process and recovery of C_3H_8 are still industrially required but challenging.[33–36]

Herein, we developed a pore-nanospace-engineering strategy to optimize the pore-nanospaces for the separation of low-concentration C_2–C_3 from CH_4 by constructing a series of UiO-66-type Zr-MOFs, UiO-66/66-Naph/66-Anth and DUT-52, in which the pore size, volume, surface and environment could be finely tuned by introducing different aromatic moieties (Fig. 1).[37–39] Noteworthily, UiO-66-Naph was demonstrated to be the best candidate, exhibiting the highest C_3H_8/CH_4 selectivity, CH_4 productivity and C_2H_6/C_3H_8 capture capacity compared to the other three Zr-MOFs, owing to its appropriately reduced pore size and rich aromaticity (extensive π-electron system), which provided multiple interaction sites for C_2H_6 and C_3H_8. Furthermore, theoretical calculations confirmed that the optimized pore nanospace and surface facilitated C–H⋯π interactions in the van der Waals (vdW) region, which play a pivotal role for the challenging separation of C_2–C_3 light hydrocarbons from CH_4.

2. Results and discussion

Synthesis, phase purity and porosity

Four Zr-MOFs, UiO-66, UiO-66-Naph, UiO-66-Anth and DUT-52, were synthesized through the solvothermal reaction of $ZrCl_4$ with the corresponding ligands H_2BDC (terephthalic acid), $H_2$1,4-NDC (1,4-naphthalenedicarboxylic acid), $H_2$9,10-ADC (9,10-anthracenedicarboxylic acid) and $H_2$2,6-NDC (2,6-naphthalenedicarboxylic acid), respectively, in *N*,*N*-dimethylformamide (DMF) with the addition of a modulator (formic acid, trifluoroacetic acid or HCl) (Fig. 1a),[32,40] forming isostructures with the *fcu*-net topology. The phase purity of the as-prepared
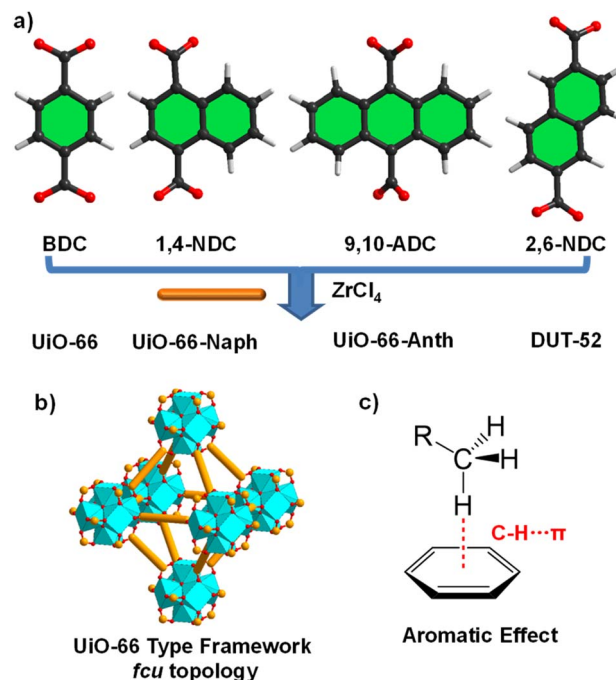

Fig. 1 (a) Ligands of the four MOFs. The green color highlights the size and direction of the aromatic systems. (b) Structure of UiO-66 type frameworks with the ligands simplified as yellow sticks. (c) Schematic representation of aromatic effect toward RCH_3 *via* C–H⋯π interaction.

bulk samples was confirmed by PXRD patterns (Fig. S1–S4 in the ESI,† respectively), matching well with the simulated patterns from reported structures.[32,39] The thermal stability of the four MOFs was assessed by thermogravimetric analysis (TGA) and variable-temperature PXRD (VT-PXRD) patterns, demonstrating that they are stable up to 400 °C except for UiO-66-Anth, which is stable up to 300 °C (Fig. S9–S13,† respectively). Moreover, the chemical stability of the four MOFs was evaluated by treating the samples in hot water (60 °C for UiO-66 and 80 °C for the other MOFs) and aqueous solutions with different pH values (6 M HCl for UiO-66/66-Naph, 0.5 M HCl for DUT-52, 1 M HCl for UiO-66-Anth, pH = 12 for UiO-66/66-Naph/66-Anth, and pH = 10 for DUT-52), and then checked by PXRD and N_2 (77 K) adsorption experiments, revealing that all the MOFs retained their structural integrity, which indicates their excellent robustness (Fig. S5–S8, S15–S18 and Table S1,† respectively).

N_2 (77 K) adsorption measurements were performed to evaluate the porosity of the four MOFs, which all presented type I microporous adsorption isotherms (Fig. 2a and S19–S22,† respectively). The Brunauer–Emmett–Teller (BET) surface areas (S_{BET}) and pore volumes follow the order of DUT-52 (1641 m² g⁻¹ and 0.70 cm³ g⁻¹) > UiO-66 (1305 m² g⁻¹ and 0.47 cm³ g⁻¹) > UiO-66-Naph (881 m² g⁻¹ and 0.40 cm³ g⁻¹) > UiO-66-Anth (676 m² g⁻¹ and 0.32 cm³ g⁻¹) (Table S4†), which is consistent with the order of the pore size distribution (PSD) calculated based on the DFT method, namely, DUT-52 (1.03 and 1.73 nm) > UiO-66 (0.86 and 1.11 nm) > UiO-66-Naph (0.55 and 1.14 nm) > UiO-66-
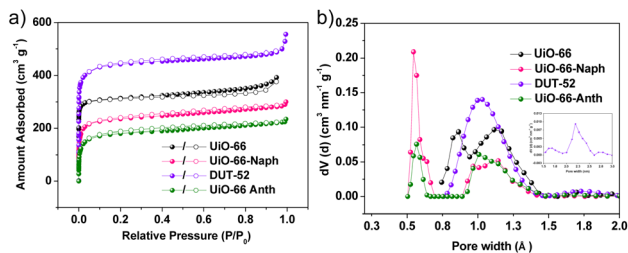
Fig. 2 (a) N$_2$ adsorption isotherms of UiO-66, UiO-66-Naph, DUT-52 and UiO-66-Anth at 77 K. Solid symbols: adsorption and open symbols: desorption. (b) Pore size distribution of the four MOFs calculated in the QSDFT mode.

Anth (0.57 and 1.01 nm), respectively. This demonstrates the effective pore-nanospace manipulation by introducing an aromatic system with different sizes and arrangements (Fig. 2b and Table S4†). It is worth noting that the introduction of more extensive π-electron systems not only endowed the UiO-66 family with more aromatic-rich pore-environment, thereby enhancing the C$_2$H$_6$/C$_3$H$_8$-framework interactions *versus* CH$_4$, but also finely tuned the pore size, pore volume and pore surface, which may impact the separation of C$_2$–C$_3$ light hydrocarbons from CH$_4$.

C$_1$–C$_3$ light hydrocarbon adsorption

To evaluate the gas separation performance, the CH$_4$, C$_2$H$_6$ and C$_3$H$_8$ adsorption isotherms were measured at 273, 283 and 298

Fig. 3 Gas adsorption and separation performance of UiO-66, UiO-66-Naph, DUT-52 and UiO-66-Anth. (a–d) CH$_4$, C$_2$H$_6$ and C$_3$H$_8$ adsorption isotherms of the MOFs at 298 K. (e) IAST selectivity of the MOFs for C$_3$H$_8$/CH$_4$ (50 : 50, v/v) at 298 K. (f) Q_{st} of C$_2$H$_6$ and C$_3$H$_8$ adsorption of the MOFs as a function of the surface coverage.

K (Fig. 3a–d and S23–S26†), respectively. All the MOFs presented much higher C$_2$H$_6$ and C$_3$H$_8$ uptake capacity than CH$_4$, indicating the preferential C$_2$H$_6$ and C$_3$H$_8$ adsorption. This can be attributed to the higher polarizability and larger kinetic size of the C$_2$H$_6$ and C$_3$H$_8$ guests, imposing stronger gas-framework interactions in the confined pore-nanospace.[41] Notably, the introduction of bulk naphthalene and anthracene in UiO-66 resulted in a reduction in amount of CH$_4$, C$_2$H$_6$ and C$_3$H$_8$ adsorption, stemming from the reduced pore volume. However, the uptake ratios of C$_2$H$_6$/CH$_4$ and C$_3$H$_8$/CH$_4$ for UiO-66, UiO-66-Naph and UiO-66-Anth were different, especially in the low-pressure region (0.05 bar), where the values for C$_2$H$_6$/CH$_4$ and C$_3$H$_8$/CH$_4$ are 12/50 for UiO-66, 16/54 for UiO-66-Naph, and 26/76 for UiO-66-Anth. These results suggest that the aromatic-functionalized MOFs may present better low-concentration C$_2$–C$_3$ light hydrocarbons separation potential from CH$_4$ after enlarging the aromatic rings, which was further confirmed by transient breakthrough experiments (*vide infra*).

The ideal adsorption solution theory (IAST) model with dual-site Langmuir–Freundlich fitting was implemented to calculate the C$_2$H$_6$/CH$_4$ and C$_3$H$_8$/CH$_4$ selectivity in different mixing ratios (Fig. 3e, S35–S37 and Table S4†).[42] For C$_2$H$_6$/CH$_4$ (10 : 90 or 50 : 50, v/v), the IAST selectivity showed a decreasing trend in the order of UiO-66-Anth ≥ UiO-66-Naph > UiO-66 > DUT-52 at 298 K and 1 bar. In the case of C$_3$H$_8$/CH$_4$ (10 : 90 or 50 : 50, v/v), the IAST selectivity presented a similar descending trend of UiO-66-Naph > UiO-66-Anth > UiO-66 > DUT-52. The above-mentioned results manifest that MOFs with a small pore size, which can be achieved by introducing condensed aromatic rings, are beneficial for improving the C$_2$H$_6$/CH$_4$ and C$_3$H$_8$/CH$_4$ adsorption selectivity, while MOFs with a larger pore size result in higher C$_2$H$_6$/C$_3$H$_8$ uptake. Noteworthily, the C$_2$H$_6$/CH$_4$ and C$_3$H$_8$/CH$_4$ (50 : 50, v/v) selectivity for UiO-66-Naph are higher than that of many reported MOF materials under ambient conditions, demonstrating that the introduction of an aromatic system with an appropriate size can effectively enhance the C$_2$–C$_3$ light hydrocarbon adsorption (Table S3†). For comparison with the many reported strategies applied to optimize the C$_1$–C$_3$ light hydrocarbon separation ability of porous materials (Table S2†), we calculated the increasing ratio of the C$_3$/C$_1$ IAST selectivity (C$_3$/C$_1$, 50 : 50) to evaluate the efficiency of these strategies. It is noteworthy that the aromatic effect is among the most effective strategies reported thus far.

The isosteric heat of adsorption (Q_{st}) for C$_2$H$_6$ and C$_3$H$_8$ was calculated based on the gas adsorption isotherms at 273, 283 and 298 K using the Clausius–Clapeyron equation (Fig. S23–S34†).[43] As depicted in Fig. 3f, the Q_{st} values at near zero coverage for C$_2$H$_6$/C$_3$H$_8$ show a clear decreasing trend from UiO-66-Naph (28.3/37.9 kJ mol^{-1}) ≈ UiO-66-Anth (28.9/35.1 kJ mol^{-1}) to UiO-66 (26.8/32.7 kJ mol^{-1}) and DUT-52 (24.6/28.9 kJ mol^{-1}), suggesting decreased gas-framework interactions. For the three MOFs with the same ligand length but different fused aromatic rings, UiO-66 has the lowest Q_{st} value, demonstrating the effectiveness of the aromatic systems, which result in an enhanced confined effect. The comparable C$_2$–C$_3$ hydrocarbon Q_{st} values of UiO-66-Anth and UiO-66-Naph imply that the introduction of an oversized aromatic system does not
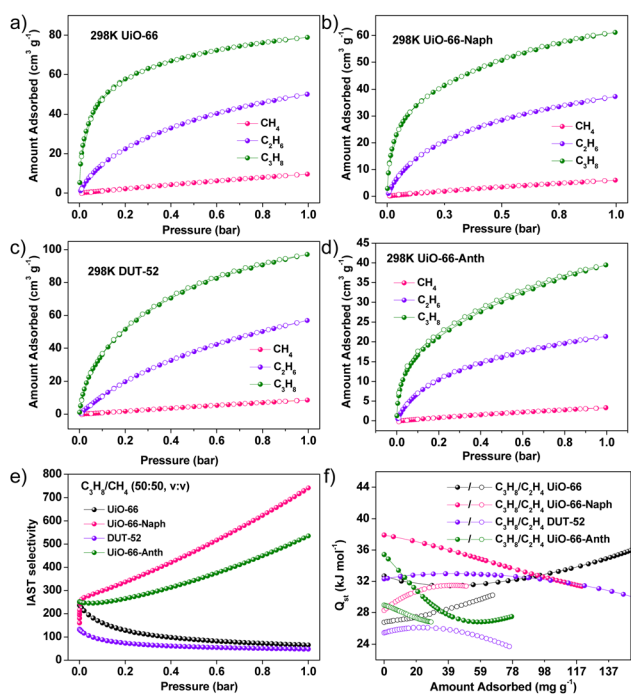
12904 | *J. Mater. Chem. A*, 2023, **11**, 12902–12909

This journal is © The Royal Society of Chemistry 2023

necessarily lead to stronger gas-framework interactions. Compared with UiO-66/66-Naph/66-Anth, DUT-52 with the largest pore size showed the lowest Q_{st} values, although it also has a larger aromatic system than UiO-66, indicating that a delicate balance between the pore size and aromatic ring size is important for the gas-framework interactions.

Theoretical calculations

Considering that the IAST selectivity calculation based on the pure-component adsorption isotherms may not be able to reflect the practical separation capacity of the C_1–C_3 gas mixture, we further investigated the gas adsorption mechanism through theoretical calculations using the grand canonical Monte Carlo (GCMC) method.[44–47] The structural models of all the MOFs were constructed based on the single-crystal structures of UiO-66 and DUT-52, respectively. It is worth noting that the benzene rings repulse each other in the simulated UiO-66-Anth structure owing to the bulky volume of anthracene, thereby resulting in a very twisted and unreasonable conformation. Thus, it is expected that UiO-66-Anth contains framework defects to some extent to reduce the density of the anthracene rings to stay in a reasonable low-energy conformation, as evidenced by the PSD (2.19 nm), solid ^{13}C NMR, and TGA (stable only up to 300 °C, lower than other Zr-MOFs) analyses (Fig. S9, S13, S14 and S44†). Consequently, the ideal structure model for UiO-66-Anth was not constructed. The density distribution results for CH_4/C_2H_6/C_3H_8 at 1 bar in the other three Zr-MOFs reveal that all three gases are primarily located in the tetrahedral cage through vdW force interactions (Fig. S46†). It can be seen that DUT-52 has more pore nanospace for gas capture than the other two Zr-MOFs. Furthermore, the gas density in the tetrahedral cage increased gradually together with an increase in the gas molecule size, indicating gradually enhanced gas-framework interactions. The calculated binding energies of CH_4, C_2H_6 and C_3H_8 for UiO-66-Naph (23.5, 33.2, and 44.6 kJ mol^{-1}) are higher than that of UiO-66 (18.9, 23.5, and 43 kJ mol^{-1}), indicating stronger gas-framework interactions, which can be attributed to the aromatic effect in the present of similar small pores (Table S5†), respectively. However, for DUT-52, its calculated CH_4 (16.8 kJ mol^{-1}) and C_3H_8 (32.8 kJ mol^{-1}) binding energies are lower than that of UiO-66, while the C_2H_6 binding energy (26.7 kJ mol^{-1}) is slightly higher than that of UiO-66. These results are consistent with the Q_{st} results, implying that large pores have a negative impact on the gas-framework interactions. Concurrently, the binding energies of C_2H_6 and C_3H_8 are much higher than that of CH_4 for all three MOFs, consistent with the experimental results, further highlighting the potential C_2–C_3 light hydrocarbon separation performance from CH_4. For all three MOFs, CH_4, C_2H_6 and C_3H_8 are grasped in their tetrahedral cage mainly through C–H···π interactions. Notably, the C–H···π interacting distances in UiO-66-Naph for all three gases are shorter than that in UiO-66, and consequently stronger gas-framework interactions existed in the former structure (Fig. 4). Specifically, the C–H···π distances in UiO-66 follow the order of CH_4 (3.84–3.87, average 3.84 Å) > C_2H_6 (3.54–3.61, average 3.57 Å) > C_3H_8 (3.11–3.42,

average 3.28 Å), that in UiO-66-Naph is CH_4 (3.18–3.71, average 3.39 Å) > C_2H_6 (3.07–3.28, average 3.17 Å) > C_3H_8 (2.95–3.70, average 3.27 Å), and that in DUT-52 is CH_4 (3.82–3.94 Å, average 3.87 Å) > C_2H_6 (3.09–3.41 Å, average 3.25 Å) > C_3H_8 (2.95–3.70 Å, average 3.39 Å).[48,49] In addition, the unconventional C–H···O hydrogen bonds appeared in UiO-66, with the values of 3.45 Å (C_2H_6) and 3.94 Å (C_3H_8). The average C–H···π distances are consistent with the calculated binding energy results. For example, all the average distances of UiO-66-Naph are shorter than the corresponding distances of UiO-66. The average distances between CH_4, C_3H_8 and DUT-52 are longer than that of UiO-66, while the distance for C_2H_6 is shorter. Overall, the theoretical calculations demonstrate that properly aligned large aromatic systems with a suitable size in the pore nanospaces not only result in a smaller pore size, but also provide more potential donors for C–H···π interactions, thus leading to enhanced C_2–C_3 light hydrocarbon separation performance from CH_4.

Breakthrough experiment

To evaluate the practical separation performance, transient breakthrough experiments were carried out for the four Zr-MOFs under ambient conditions, in which the CH_4/C_2H_6/C_3H_8 (85 : 10 : 5, v/v/v) mixture flowed over a fixed-bed column at a flow rate of 5 mL min^{-1} (Fig. 5a–d and Table S4†), respectively. For all four MOFs, high-grade CH_4 (UiO-66 > 98.7%, UiO-66-Naph > 99.6%, DUT-52 > 95.6%, UiO-66-Anth > 91.4%) was first eluted, whereas C_2H_6 and C_3H_8 were retained in the fixed-bed column for a certain time, and then eluted one after the other. The retention time of C_2H_6 is similar for UiO-66, UiO-66-Naph and DUT-52, while that for UiO-66-Anth is significantly short. Alternatively, the retention time of C_3H_8 showed a decreasing trend of UiO-66-Naph > UiO-66 > DUT-52 ≫ UiO-66-Anth. The high-grade CH_4 productivity for UiO-66-Naph is 2.25 mmol g^{-1}, which is obviously higher than that for UiO-66 (1.65 mmol g^{-1}), DUT-52 (2.08 mmol g^{-1}) and UiO-66-Anth (0.17 mmol g^{-1}), suggesting the better low-concentration C_2–C_3 hydrocarbon separation potential of UiO-66-Naph. Surprisingly, the C_2H_6 (0.18 mmol g^{-1}) and C_3H_8 (0.77 mmol g^{-1}) capture capacity by UiO-66-Naph is slightly higher than that by UiO-66 (C_2H_6: 0.17 mmol g^{-1} and C_3H_8: 0.74 mmol g^{-1}), and even comparable with that of DUT-52 (C_2H_6: 0.28 mmol g^{-1} and C_3H_8: 0.63 mmol g^{-1}), although the surface area and pore volume of UiO-66-Naph are significantly smaller than that of UiO-66 and DUT-52, which also contradict the uptake capacity measured from the single-gas adsorption isotherms (Fig. 3a–c). This indicates that the aromatic effect plays a significant role in the practical separation of the ternary CH_4/C_2H_6/C_3H_8 (85 : 10 : 5, v/v/v) gas mixture with a low concentration of C_2H_6 and C_3H_8, endowing UiO-66-Naph containing a larger aromatic system with much more efficient utilization of its pore nanospaces to take up low-concentrated C_2H_6 and C_3H_8 gases from the gas mixture. In contrast, UiO-66-Anth with the largest aromatic system exhibited the shortest C_2/C_3 retention time, the lowest CH_4 production (0.17 mmol g^{-1}) and the lowest C_2/C_3 capture amount (0.15/0.29 mmol g^{-1}). The reason for this may be that

This journal is © The Royal Society of Chemistry 2023

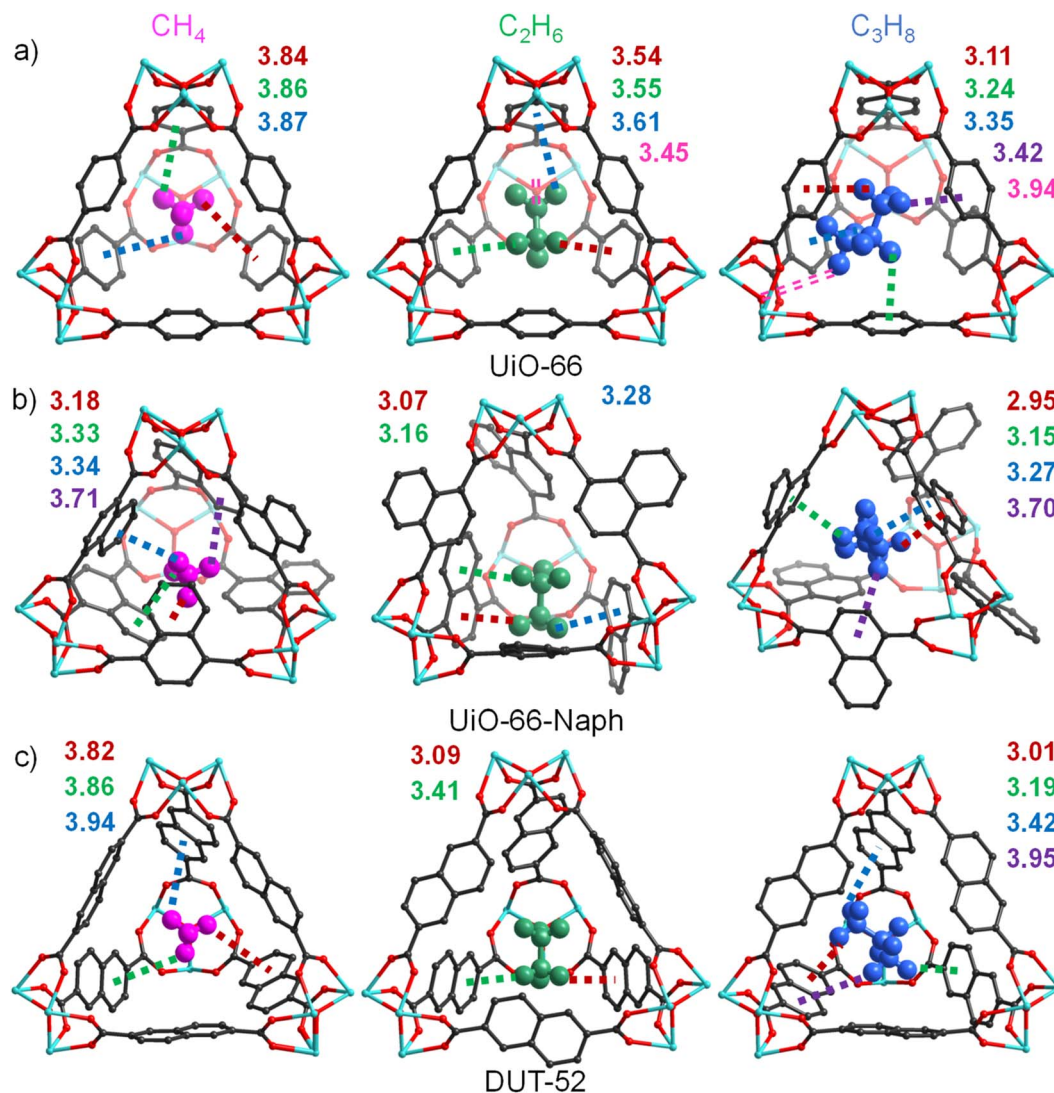*J. Mater. Chem. A*, 2023, **11**, 12902–12909 | **12905**

Fig. 4 GCMC-simulated primary absorption sites of $CH_4/C_2H_6/C_3H_8$ in (a) UiO-66, (b) UiO-66-Naph and (c) DUT-52. Dotted line, C–H···π interaction; double dotted line, C–H···O interaction. The hydrogen atoms of the MOFs have been omitted for clarity.

the too small pore size and low pore volume of UiO-66-Anth limit the gas diffusion in the dynamic separation processes, resulting in low gas capture and quick breakthrough. Moreover, the inevitable formation of framework defects due to the steric repulsion between the bulky anthracene rings is detrimental to the validity of the aromatic effect. Alternatively, DUT-52 with the largest pore size and volume showed the worst C_2/C_1 and C_3/C_1 selectivity, adsorption Q_{st} and C_3 capture capacity. Although its CH_4 productivity was better than UiO-66 and C_2 capture capacity better than UiO-66-Naph, the overall C_2/C_3 retention times were not improved compared with UiO-66-Naph. Therefore, it can be concluded that pore engineering with an appropriate aromatic system is an important factor in the dynamic gas separation process of the ternary $C_3H_8/C_2H_6/CH_4$ mixture, depending on the trade-off of the pore size and aromatic ring size. To better assess the C_3H_8/CH_4 separation performance from the ternary $CH_4/C_2H_6/C_3H_8$ gas mixture, the separation potential (Δq) was calculated based on the transient breakthrough experiments, in which UiO-66-Naph presented the highest Δq value of 0.75 mmol g^{-1} compared with UiO-66 (0.71 mmol g^{-1}), DUT-52 (0.61 mmol g^{-1}) and UiO-66-Anth (0.2 mmol g^{-1}), further suggesting the aromatic effect (for the calculation details, see Section S7 in the ESI†). Multiple transient breakthrough experiments on the four MOFs were conducted, which revealed almost the same gas retention time as the first breakthrough curve, suggesting their excellent durability and recyclability (Fig. S38–S41,† respectively).

To evaluate their regeneration potential, an He stream with a rate 5 mL min^{-1} was flowed over the packing column at 100 °C, while the composition of the eluted gas was monitored by a gas chromatograph. As shown in Fig. 5e, f, S42 and S43,† UiO-66-Naph can be fully activated after 70 min, even shorter than UiO-66 (120 minutes) and comparable with DUT-52, indicating a low regeneration energy requirement, which is beneficial for practical industrial application. This implies that the enhanced aromatic effect in UiO-66-Naph has little influence on the
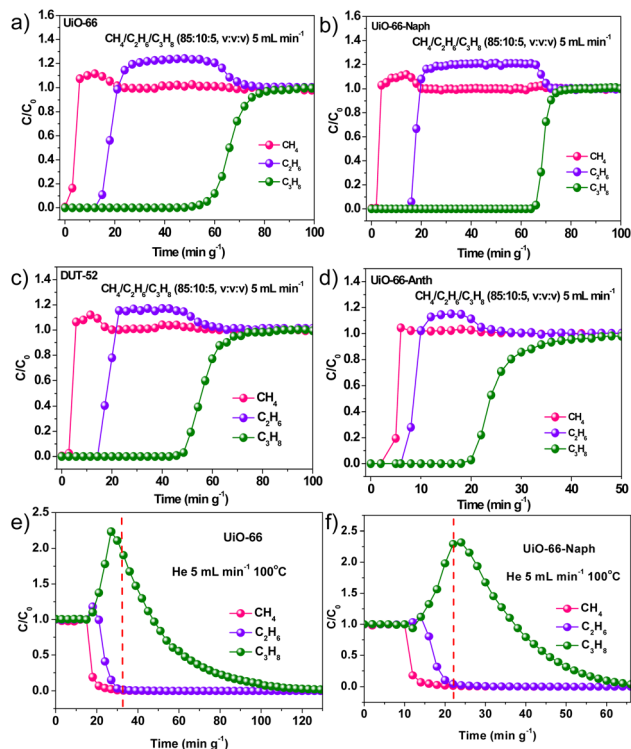
12906 | *J. Mater. Chem. A*, 2023, **11**, 12902–12909

This journal is © The Royal Society of Chemistry 2023

Fig. 5 Transient breakthrough curves (a–d) of $CH_4/C_2H_6/C_3H_8$ (85 : 10 : 5, v/v/v) mixture for UiO-66, UiO-66-Naph, DUT-52 and UiO-66-Anth, and desorption curves (e and f) for UiO-66 and UiO-66-Naph, respectively.

desorption of $CH_4/C_2H_6/C_3H_8$ gases, which may be related with the decrease in the Q_{st} values when more C_2H_6 and C_3H_8 gas molecules are adsorbed in UiO-66-Naph (Fig. 3f). It should be noted that high-grade C_3H_8 (UiO-66 > 99.5%, UiO-66-Naph > 99.1%, DUT-52 > 96.2%, UiO-66-Anth > 96.0%) can be afforded after the CH_4 and C_2H_6 off-gases are eluted completely.

3. Conclusion

In summary, we demonstrated that a properly functionalized UiO-66 topological MOF, UiO-66-Naph, featuring optimized pore nanospaces by virtue of the introduction of a naphthalene moiety in the linear carboxylic acid, exhibited efficient low-concentration C_2–C_3 light hydrocarbon separation from a ternary $CH_4/C_2H_6/C_3H_8$ gas mixture. The experimental and simulation results from four isostructural Zr-MOFs with systematic modification of the pore environment by aromatic rings of different sizes revealed that the introduction of a bulky aromatic system with suitable size in the UiO-66 framework not only effectively reduced the pore size, but also provided a more aromatic-rich pore environment, thereby leading to a significantly enhanced separation performance for the low-concentrated C_2–C_3 light hydrocarbons from CH_4. In addition, the excellent physical and chemical stability of UiO-66-Naph guarantee adequate ability for practical separation application. Compared with its UiO-66, DUT-52 and UiO-66-Anth analogues, UiO-66-Naph presented better C_2/C_1 and C_3/C_1

selectivity, CH_4 productivity, C_3H_8 capture capacity, and the longest C_2/C_3 retention time, facilitated by the stronger C–H···π interactions and pore confinement. Moreover, its easy regeneration ability comparable with DUT-52 with larger pores and better than UiO-66 suggests a lower regeneration energy requirement, further highlighting that the bulky aromatic-functionalized UiO-66-Naph is a promising adsorbent for the separation of the ternary $CH_4/C_2H_6/C_3H_8$ gas mixture. This work can provide guidelines for the design of new porous solid adsorbents in the challenging gas adsorption and separation field.

4. Experimental

General procedure

The standard synthesis procedure was performed by dissolving zirconium tetrachloride and carboxylate ligands in *N,N*-dimethylformamide (DMF) at room temperature in a 20 mL glass vial, followed by the addition of a modulator.[28,29,39] The as-obtained mixture was sealed and placed in a pre-heated oven at 120 °C for a few days. Crystallization was carried out under static conditions. After cooling in air to room temperature, the resulting crystals were filtered and repeatedly washed with DMF.

Synthesis of UiO-66

A mixture of *p*-phthalic acid (0.083 g, 0.5 mmol) and zirconium tetrachloride (0.12 g, 0.5 mmol) was dissolved in formic acid (3.5 mL) and DMF (16.5 mL). After stirring for 10 min, this solution was transferred to a 40 mL glass vial and kept at 120 °C for 5 days. After cooling to room temperature, the resulting crystals were obtained and washed repeatedly with acetone.

Synthesis of UiO-66-Naph

A mixture of 1,4-naphthalenedicarboxylic acid ($H_2$1,4-NDC, 0.11 g, 0.5 mmol) and zirconium tetrachloride (0.12 g, 0.5 mmol) was dissolved in trifluoroacetic acid (1.5 mL) and DMF (18.5 mL). After stirring for 10 min, this solution was transferred to a 40 mL glass vial and kept at 120 °C for 5 days. After cooling to room temperature, the resulting crystals were obtained and washed repeatedly with acetone.

Synthesis of DUT-52

A mixture of 2,6-naphthalenedicarboxylic acid ($H_2$2,6-NDC, 0.11 g, 0.5 mmol) and zirconium tetrachloride (0.12 g, 0.5 mmol) was dissolved in concentrated HCl (0.5 mL) and DMF (19.5 mL). After stirring for 10 min, the solution was transferred to a 40 mL glass vial and kept at 120 °C for 5 days. After cooling to room temperature, the resulting crystals were obtained and washed repeatedly with acetone.

Synthesis of UiO-66-Anth

A mixture of 9,10-anthracenedicarboxylic acid (9,10-ADC, 0.15 g, 0.5 mmol) and zirconium tetrachloride (0.12 g, 0.5 mmol) was dissolved in trifluoroacetic acid (1.5 mL) and DMF (18.5 mL).

This journal is © The Royal Society of Chemistry 2023

J. Mater. Chem. A, 2023, **11**, 12902–12909 | **12907**

After stirring for 10 min, the solution was transferred to a 40 mL glass vial and kept at 120 °C for 5 days. After cooling to room temperature, the resulting crystals were obtained and washed repeatedly with acetone.

Author contributions

Zhang-Wen Wei and Cheng-Yong Su directed the research projects and supervised the work, as well as contributed to funding acquisition; Xiao-Hong Xiong designed and planned the study; Liang Zhang conducted the experiments and finished formal analysis; the original draw was written by Liang Zhang and Cheng-Xia Chen; Liu-Li Meng and Lu-Zhu Qin revised the manuscript and provided valuable suggestions. All authors discussed the results and contributed to the paper.

Conflicts of interest

There are no conflicts to declare.

Notes and references

1 G. George, N. Bhoria, S. AlHallaq, A. Abdala and V. Mittal, *Sep. Purif. Technol.*, 2016, **158**, 333–356.
2 T. Tian, Z. Zeng, D. Vulpe, M. E. Casco, G. Divitini, P. A. Midgley, J. Silvestre-Albero, J.-C. Tan, P. Z. Moghadam and D. Fairen-Jimenez, *Nat. Mater.*, 2018, **17**, 174–179.
3 Y. He, W. Zhou, G. Qian and B. Chen, *Chem. Soc. Rev.*, 2014, **43**, 5657–5678.
4 T. A. Makal, J.-R. Li, W. Lu and H.-C. Zhou, *Chem. Soc. Rev.*, 2012, **41**, 7761–7779.
5 Y. He, R. Krishna and B. Chen, *Energy Environ. Sci.*, 2012, **5**, 9107–9120.
6 J. A. Mason, M. Veenstra and J. R. Long, *Chem. Sci.*, 2014, **5**, 32–51.
7 X. Zhang, L. Li, J.-X. Wang, H.-M. Wen, R. Krishna, H. Wu, W. Zhou, Z.-N. Chen, B. Li, G. Qian and B. Chen, *J. Am. Chem. Soc.*, 2020, **142**, 633–640.
8 T. Kundu, M. Wahiduzzaman, B. B. Shah, G. Maurin and D. Zhao, *Angew. Chem., Int. Ed.*, 2019, **58**, 8073–8077.
9 Z. Niu, X. Cui, T. Pham, P. C. Lan, H. Xing, K. A. Forrest, L. Wojtas, B. Space and S. Ma, *Angew. Chem., Int. Ed.*, 2019, **58**, 10375.
10 P. Guo, M. Chang, T. Yan, Y. Li and D. Liu, *Chin. J. Chem. Eng.*, 2022, **42**, 10–16.
11 K. Jiang, L. Zhang, T. Xia, Y. Yang, B. Li, Y. Cui and G. Qian, *Sci. China Mater.*, 2019, **62**, 1315–1322.
12 J. Li, X. Luo, N. Zhao, L. Zhang, Q. Huo and Y. Liu, *Inorg. Chem.*, 2017, **56**, 4141–4147.
13 J. Jia, L. Wang, F. Sun, X. Jing, Z. Bian, L. Gao, R. Krishna and G. Zhu, *Chem.–Eur. J.*, 2014, **20**, 9073–9080.
14 P. Deria, D. A. Gómez-Gualdrón, W. Bury, H. T. Schaef, T. C. Wang, P. K. Thallapally, A. A. Sarjeant, R. Q. Snurr, J. T. Hupp and O. K. Farha, *J. Am. Chem. Soc.*, 2015, **137**, 13183–13190.
15 S. J. Geier, J. A. Mason, E. D. Bloch, W. L. Queen, M. R. Hudson, C. M. Brown and J. R. Long, *Chem. Sci.*, 2013, **4**, 2054–2061.
16 Z. Chen, P. Li, R. Anderson, X. Wang, X. Zhang, L. Robison, L. R. Redfern, S. Moribe, T. Islamoglu, D. A. Gómez-Gualdrón, T. Yildirim, J. F. Stoddart and O. K. Farha, *Science*, 2020, **368**, 297–303.
17 L. Wang, W. Zhang, J. Ding, L. Gong, R. Krishna, Y. Ran, L. Chen and F. Luo, *Nano Res.*, 2022, DOI: 10.1007/s12274-022-4915-0.
18 R.-B. Lin, S. Xiang, W. Zhou and B. Chen, *Chem*, 2020, **6**, 337–363.
19 W. G. Cui, T. L. Hu and X. H. Bu, *Adv. Mater.*, 2020, **32**, e1806445.
20 J. Pang, F. Jiang, M. Wu, C. Liu, K. Su, W. Lu, D. Yuan and M. Hong, *Nat. Commun.*, 2015, **6**, 7575.
21 R. Augelletti, M. Conti and M. C. Annesini, *J. Cleaner Prod.*, 2017, **140**, 1390–1398.
22 M. J. Ahmed and S. K. Theydan, *J. Nat. Gas Sci. Eng.*, 2014, **18**, 1–6.
23 G. S. Cheripally, A. Mannava, G. Kumar, R. Gupta, P. Saha, B. Mandal, R. Uppaluri, S. Gumma and A. K. Ghoshal, *J. Chem. Eng. Data*, 2013, **58**, 1606–1612.
24 Y. Zhang, L. Yang, L. Wang, S. Duttwyler and H. Xing, *Angew. Chem., Int. Ed.*, 2019, **58**, 8145–8150.
25 H.-F. Zhang, M. Li, X.-Z. Wang, D. Luo, Y.-F. Zhao, X.-P. Zhou and D. Li, *J. Mater. Chem. A*, 2018, **6**, 4260–4265.
26 C. X. Chen, Z. W. Wei, J. J. Jiang, S. P. Zheng, H. P. Wang, Q. F. Qiu, C. C. Cao, D. Fenske and C. Y. Su, *J. Am. Chem. Soc.*, 2017, **139**, 6034–6037.
27 Y. Chen, D. Lv, J. Wu, J. Xiao, H. Xi, Q. Xia and Z. Li, *Chem. Eng. J.*, 2017, **308**, 1065–1072.
28 S. Xian, J. Peng, Z. Zhang, Q. Xia, H. Wang and Z. Li, *Chem. Eng. J.*, 2015, **270**, 385–392.
29 H. F. Drake, Z. Xiao, G. S. Day, S. W. Vali, L. L. Daemen, Y. Cheng, P. Cai, J. E. Kuszynski, H. Lin, H.-C. Zhou and M. R. Ryder, *ACS Appl. Mater. Interfaces*, 2022, **14**, 11192–11199.
30 C. Jiang, X. Wang, Y. Ouyang, K. Lu, W. Jiang, H. Xu, X. Wei, Z. Wang, F. Dai and D. Sun, *Nanoscale Adv.*, 2022, **4**, 2077–2089.
31 J. Pang, C. T. Lollar, S. Che, J.-S. Qin, J. Li, P. Cai, M. Wu, D. Yuan, M. Hong and H.-C. Zhou, *CCS Chem.*, 2021, **3**, 1701–1709.
32 J. H. Cavka, S. Jakobsen, U. Olsbye, N. Guillou, C. Lamberti, S. Bordiga and K. P. Lillerud, *J. Am. Chem. Soc.*, 2008, **130**, 13850–13851.

12908 | *J. Mater. Chem. A*, 2023, **11**, 12902–12909

This journal is © The Royal Society of Chemistry 2023

33 Y. Xiong, T. Yang, S. Chen, C.-H. Zhang, C.-X. Chen, Z.-W. Wei, D. Wang, J.-J. Jiang and C.-Y. Su, *Cryst. Growth Des.*, 2019, **19**, 300–304.

34 D. Wang, T. Zhao, Y. Cao, S. Yao, G. Li, Q. Huo and Y. Liu, *Chem. Commun.*, 2014, **50**, 8648–8650.

35 Y. Chen, Z. Qiao, D. Lv, H. Wu, R. Shi, Q. Xia, H. Wang, J. Zhou and Z. Li, *Ind. Eng. Chem. Res.*, 2017, **56**, 4488–4495.

36 S. Gao, C. G. Morris, Z. Lu, Y. Yan, H. G. W. Godfrey, C. Murray, C. C. Tang, K. M. Thomas, S. Yang and M. Schröder, *Chem. Mater.*, 2016, **28**, 2331–2340.

37 X. Wang, L. Li, Y. Wang, J.-R. Li and J. Li, *CrystEngComm*, 2017, **19**, 1729–1737.

38 G. Han, K. Wang, Y. Peng, Y. Zhang, H. Huang and C. Zhong, *Ind. Eng. Chem. Res.*, 2017, **56**, 14633–14641.

39 V. Bon, I. Senkovska, M. S. Weiss and S. Kaskel, *CrystEngComm*, 2013, **15**, 9572–9577.

40 P. M. Schoenecker, C. G. Carson, H. Jasuja, C. J. J. Flemming and K. S. Walton, *Ind. Eng. Chem. Res.*, 2012, **51**, 6513–6519.

41 J.-R. Li, R. J. Kuppler and H.-C. Zhou, *Chem. Soc. Rev.*, 2009, **38**, 1477–1504.

42 K. S. Walton and D. S. Sholl, *AIChE J.*, 2015, **61**, 2757–2762.

43 J. L. C. Rowsell and O. M. Yaghi, *J. Am. Chem. Soc.*, 2006, **128**, 1304–1315.

44 *Accelrys Materials Studio Release Motes, Release 5.5.1*, Accelrys Software, Inc., San Diego, 2010.

45 L. Valenzano, B. Civalleri, S. M. Chavan, S. Bordiga, M. Nilsen, S. Jakobsen, K. Lillerud and C. Lamberti, *Chem. Mater.*, 2011, **23**, 1700–1718.

46 L. Gong, Y. Ye, Y. Liu, Y. Li, Z. Bao, S. Xiang, Z. Zhang and B. Chen, *ACS Appl. Mater. Interfaces*, 2022, **14**, 19623–19628.

47 M. Fischer, F. Hoffmann and M. Fröba, *ChemPhysChem*, 2010, **11**, 2220–2229.

48 D. Lv, Z. Liu, F. Xu, H. Wu, W. Yuan, J. Yan, H. Xi, X. Chen and Q. Xia, *Sep. Purif. Technol.*, 2021, **266**, 118198.

49 Y. Zhang, L. Yang, L. Wang, X. Cui and H. Xing, *J. Mater. Chem. A*, 2019, **7**, 27560–27566.

This journal is © The Royal Society of Chemistry 2023

J. Mater. Chem. A, 2023, **11**, 12902–12909 | **12909**